# Conductivity and Susceptibility Mapping Using Broadband Electromagnetic Sensors

Haoping Huang and I.J. Won
Geophex, Ltd, 605 Mercury Street, Raleigh, N.C. 27603-2343

## ABSTRACT

The apparent conductivity and apparent magnetic permeability are derived from broadband electromagnetic data using a conductive and magnetic half-space model. The apparent permeability is first estimated from the inphase and quadrature (or amplitude and phase) data at a low frequency. This is followed by the computation of the apparent conductivity at each frequency, using the pre-computed apparent permeability. The apparent conductivity may be computed from broadband data using five different algorithms. In general, three of the five methods yield a unique solution; the three yielding a unique solution are the apparent conductivity defined from inphase, phase, or phase-amplitude.

A suite of synthetic data based on two-layer models is presented and it is concluded that the phase-amplitude approach is the preferred method. The apparent permeability is virtually independent of the conductivity contrast at low induction numbers. However, the permeability contrast affects the apparent conductivity, especially when a resistive layer overlays a conductive basement. The field data examples show the usefulness of the broadband electromagnetic data and the resultant frequency-dependent conductivity-permeability maps for characterizing complex environmental sites.

## Introduction

New broadband electromagnetic (EM) sensors have been used to detect landfills, unexploded ordnance, buried drums, trench boundaries, contaminant plumes, underground facilities, and for other applications (Keiswetter *et al.,* 1997; Keiswetter and Won, 1997; Murray and Keiswetter, 1998; Sternberg and Birken, 1999; Witten, and Calvert, 1999; Won *et al.,* 1996, 1997, 1998). In such applications, interpretation is commonly based on analysis of the measured inphase and quadrature ppm components and mapping of apparent conductivity derived from a single component of the EM responses (Won *et al.,* 1996, 1997).

Apparent conductivity is defined as the conductivity of a homogeneous half-space that produces the same response as measured over the real earth with the same sensor. Apparent conductivity is a parameter which, in general, is related to target electrical properties and has units of conductivity, whereas the measured inphase and quadrature responses (ppm) are dimensionless numbers which are not intuitively related to the physical parameters of the earth. Apparent conductivity presentation is a kind of normalization of the EM data; it makes data analysis and interpretation easier for both geophysicists and other scientists. If the earth were truly homogeneous, the apparent conductivity would be the same at all frequencies and equal the true earth conductivity. Moreover, quadrature data are proportional to the ground conductivity in the low to mid induction numbers, but are inversely proportional to the conductivity at mid to high induction numbers. Thus, it may occur that a moderate conductor produces a strong quadrature anomaly, whereas a good conductor produces a weak anomaly or no anomaly, in which case, inphase data have to be used to further analyze the data. Raw EM data contain many non-target anomalies (geologic noise) such as variations in thickness of conductive overburden, which could generate an anomaly more pronounced than a target anomaly. Apparent conductivity presentations generally suppress geologic noise, and target anomalies may be enhanced. If a conductive target is small in size or deeply buried, its EM response will be relatively weak so it may not be detected by using the EM data only. However, its apparent conductivity would be high enough to be identified.

The apparent conductivity may be converted from either the inphase or quadrature response as described by Won *et al.* (1996, 1997). However, the apparent conductivity can be defined in a number of ways, based on the choice of input EM data components, as reviewed by Huang and Fraser (2000). All algorithms of various definitions yield the true conductivity when the earth is a true homogeneous half-space, but yield different values of apparent conductivity when the earth is inhomogeneous. Also, the EM response may be affected by magnetic polarization, resulting in distortion of apparent conductivity in magnetic environments. Some authors have discussed the magnetic effect on EM data (*e.g.,* Huang and Fraser, 1998, 2000), indicating the need for a conductivity transformation in magnetic environments to be performed based on a magnetic permeability transformation (as the above authors did for helicopter EM data).

In this paper, we use the method similar to that of

Huang and Fraser (1998, 2000) and develop the transform algorithms for multi-frequency EM sensors, using a magnetic and conductive half-space model. The apparent conductivity can be obtained from different algorithms, based on the choice of input data components. Using synthetic data, we compare the apparent conductivities obtained from each algorithm and choose the best one to be used in practice. Finally, we present field examples from GEM-2 surveys.

## EM Response over a Homogeneous Half-Space

The EM response of a half-space for vertical magnetic dipole excitation is given by Frischknecht (1967), Ward (1967), and Ward and Hohmann (1988), among others. If the horizontal coplanar transmitting and receiving coils are at a height h above a homogeneous half-space, the secondary magnetic field $H_s$, normalized by the primary field $H_0$ at the receiving coil, is

$$\frac{H_s}{H_0} = s^3 \int_0^\infty R(\lambda)\lambda^2 \exp(-2\lambda h) J_0(\lambda s)\, d\lambda, \qquad (1)$$

where s is the coil separation and $J_0$ the Bessel function of the first kind of order zero. The term $R(\lambda)$ can be written as

$$R(\lambda) = \frac{\lambda - u_1}{\lambda + u_1} \qquad (2)$$

where $u_1$ for a homogeneous half-space is

$$u_1 = \frac{\sqrt{\lambda^2 + i\omega\sigma\mu}}{\mu_r} \qquad (3)$$

and where $\omega$ is the angular frequency, $\sigma$ is the conductivity, $\mu_r$ is the relative magnetic permeability $\mu/\mu_0$ where $\mu$ is the magnetic permeability of the earth, and $\mu_0$ is the magnetic permeability of free space. The above equations make the common quasistatic assumption that conduction currents are much larger than displacement currents, *i.e.*, $\sigma >> \omega\epsilon$ where $\epsilon$ is the dielectric permittivity.

The complex quantity $H_s/H_0$ when multiplied by $10^6$ is in units of parts per million (ppm) and consists of the real (inphase; I) and imaginary (quadrature; Q) components. Figure 1 shows I and Q as functions of $\sigma\mu f$ for various values of $\mu_r$ for the horizontal coplanar coil configuration with s = 1.66 m at one meter height over a homogeneous half-space. The effect of a magnetic permeability $\mu$ greater than $\mu_0$ is twofold. First, the permeability increases the value of $\sigma\mu f$. Secondly, as $\sigma\mu f \to 0$, the response becomes dominated by the magnetization effect, which is inphase with, and in the same direction as, the primary field. This is the induced magnetization that occurs for an alternating magnetic field of a coil just as it does for the static magnetic field of the earth. At low induction numbers, the inphase component of the response becomes frequency independent, and the quadrature component goes to zero. The inphase shift saturates when $\mu_r$ is greater than 100 (a much larger value than any geologic material, but common to man-made ferrous metal). At the other extreme, when the number $\sigma\mu f$ is large, the induced conductive response overwhelms the magnetization effect. All curves in Fig. 1 converge to that for $\mu_r = 1$ as $\sigma\mu f \to \infty$. For mid-range induction numbers, the magnetization effect and conductive effect are mixed.

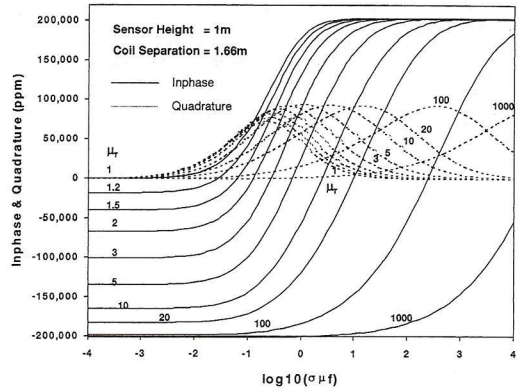


**Figure 1. Inphase I and quadrature Q components of the response of a homogeneous half-space plotted as a function of $\sigma\mu f$ for various values of the relative magnetic permeability $\mu_r$, for the horizontal coplanar coil configuration.**

Alternately, the EM response can also be expressed as amplitude $A = (I^2+Q^2)^{1/2}$ and phase angle $\alpha$ = atan(Q/I) as shown in Fig. 2. The phase angle $\alpha$ and the amplitude A are plotted as functions of $\sigma\mu f$ for various values of $\mu_r$ for the horizontal coil configuration over a homogeneous half-space. Such nomograms can be used to obtain the apparent conductivity at a particular frequency, given the permeability.

## Computation of Apparent Permeability and Conductivity

The apparent susceptibility $\kappa_a = \mu_{ra} - 1$ could be obtained from the measured magnetic data by computing the apparent permeability. However, the earth's static magnetic field samples the earth quite differently to an alternating dipole field of the transmitting coil. Static permanent magnetism may also distort susceptibility values derived assuming only induced magnetization. Apparent susceptibility, derived from the EM data, may yield more information on near-surface magnetic objects. Consequently, we prefer to obtain the apparent permeability or susceptibility

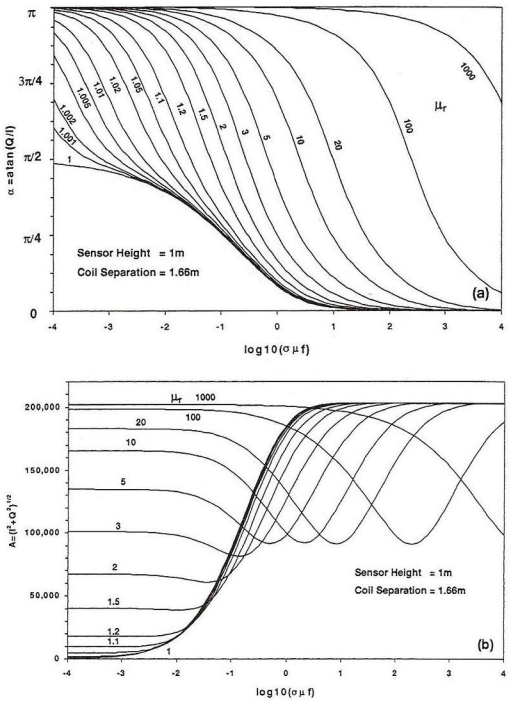


**Figure 2. (a) Phase angle and (b) amplitude of the response of a homogeneous half-space plotted as a function of $\sigma\mu f$ for various values of the relative magnetic permeability $\mu_r$, for the horizontal coplanar coil configuration.**

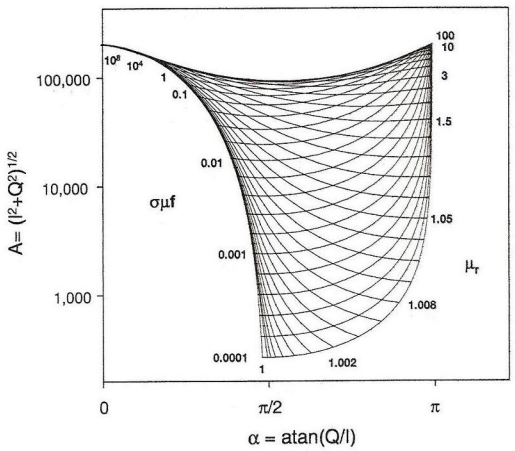


**Figure 3. The diagram of phase angle $\alpha$ and amplitude $A$ for the half-space model of a magnetic and conductive earth for several values of $\sigma\mu f$ and relative permeability $\mu_r$.**

from the raw EM data, *i.e.,* the inphase and quadrature, which are equivalent to amplitude A and phase $\alpha$. The apparent permeability is given by

$$\mu_a = f(A, \alpha). \tag{4}$$

The algorithm is illustrated in Fig. 3, which yields both relative permeability $\mu_r$ and $\sigma\mu f$. It can be seen that the permeability $\mu_r$ can be well resolved when $\sigma\mu f << 0.1$, and resolvability will be significantly reduced when $\sigma\mu f > 0.1$. The quantity $\sigma\mu f$ serves as an indication of the resolvability of the relative permeability $\mu_r$. If $\sigma\mu f$ is low, the value of $\mu_r$ from Fig. 3 is likely to be reliable. If $\sigma\mu f$ is greater than 0.1, the measured relative permeability $\mu_r$ will not be reliable.

The permeability determination depends only upon the amplitude A or the inphase I of the response as $\sigma\mu f \rightarrow 0$, as shown in Figs. 1 and 2(b); this occurs when there are no conduction currents. Thus, the magnetic permeability may be determined from the negative inphase response, which is valid when the quadrature response is zero, *i.e.,* when negligible eddy currents are induced in the earth at the transmitted frequency. The algorithm then reduces to

$$\mu_a = f(I), \qquad \text{as } \sigma\mu f \rightarrow 0. \tag{5}$$

If the earth were a truly homogeneous half-space, the relative magnetic permeability $\mu_r$ obtained from Fig. 3 would be the true relative permeability, otherwise it would be the apparent relative permeability. In practice, the above procedure should be followed using the lowest frequency data to ensure that $\sigma\mu f$ is as low as possible so as to maximize the ratio of magnetic response to conductive response.

Given the relative magnetic permeability $\mu_r$, the apparent conductivity can be determined from the inphase I, quadrature Q, phase $\alpha$, amplitude A, or both phase $\alpha$ and amplitude A (equivalent to inphase and quadrature) for each individual frequency. Therefore, there are five homogeneous half-space models based on the choice of input to an algorithm, which yields an apparent conductivity. These models are:

$$\sigma_a = \begin{Bmatrix} f(I, \mu_r) \\ f(Q, \mu_r) \\ f(\alpha, \mu_r) \\ f(A, \mu_r) \\ f(A, \alpha, \mu_r) \end{Bmatrix}, \tag{6}$$

where $\sigma_a$ is the apparent conductivity, and $\mu_r$ is obtained using Eq. 4 (Eq. 5 if $\sigma\mu f \rightarrow 0$). The five half-space models were developed originally by Fraser (1978) for helicopter

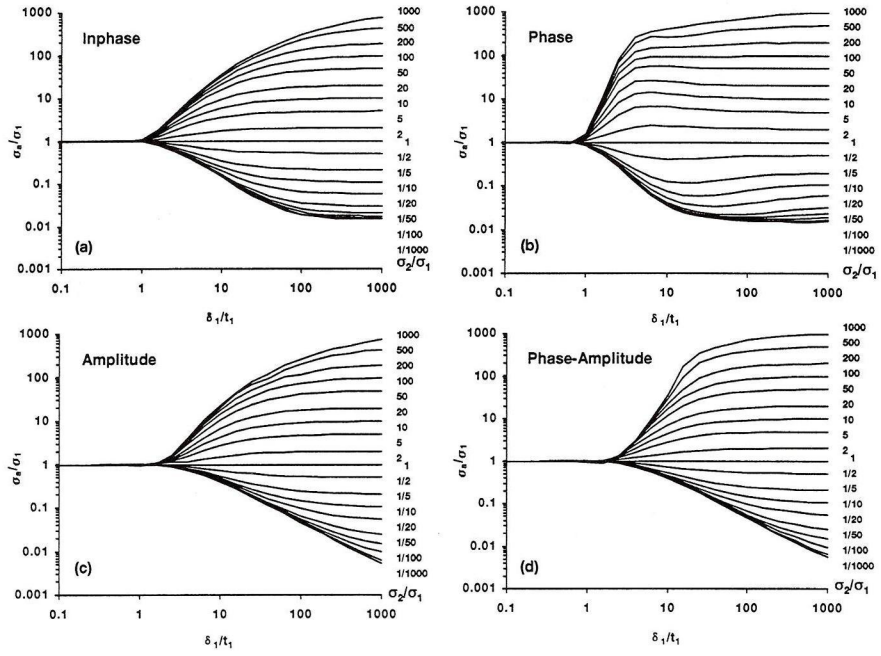


**Figure 4. The apparent conductivity curves for a suite of two-layer models for the conductivity ratios $\sigma_2/\sigma_1$ from 0.001 to 1,000. The panels are (a) *inphase conductivity,* (b) *phase conductivity,* (c) *amplitude conductivity,* and (d) *phase-amplitude conductivity.***

EM systems. He assumed that the magnetic permeability of earth is the same as free space. The *inphase* model is sensitive to ground conductivity at an intermediate value of $\sigma\mu f$, as shown in Fig. 1. There will be no solution to conductivity when $\sigma\mu f$ is either very low or very high. The *quadrature* model yields two solutions to the apparent conductivity because the quadrature response peaks at an intermediate value of $\sigma\mu f$, and the conductivity is poorly defined around the peak (Fig. 1). It should be noted that in geologic applications, the values of $\sigma\mu f$ are invariably low even at the highest frequencies, but when manmade targets are encountered, they are often very high. The *phase* model has a unique solution to conductivity, but it is insensitive to ground conductivity when the phase angle approaches to 0 and $\pi$ as can be seen in Fig. 2(a). The *amplitude* model of Fig. 2(b) yields a unique apparent conductivity solution when $\mu_r$ is less than 1.5, but as the magnetic permeability increases, there are two solutions to the apparent conductivity because the amplitude has a minimum at intermediate values of $\sigma\mu f$. The *phase-amplitude* model shown in Fig. 3 yields a unique apparent conductivity, and it is sensitive at low-intermediate values of $\sigma\mu f$.

If the earth is truly homogeneous, the conductivity obtained from any of the above equations is identical and equal to the true conductivity $\sigma$. Otherwise, it would be the apparent conductivity $\sigma_a$, and each approach would produce different results. This is expected because the geometry of the inphase current distribution in the ground is different from that of the quadrature current distribution. These different current distributions lead to different values for the homogeneous half-space apparent conductivities.

## Test on Theoretical Data

We refer below to the apparent conductivity obtained from the inphase as the *inphase conductivity,* that from the phase as the *phase conductivity,* that from the amplitude as *amplitude conductivity,* and that from the phase-amplitude as the *phase-amplitude conductivity.* We exclude the *quadrature conductivity* because it is double-valued. We compare the apparent permeability and apparent conductivity for a suite of two-layer models.

Let us first consider the behavior of the apparent conductivity for a suite of two-layer models with the magnetic permeability of free-space. Figure 4 shows the apparent conductivity curves as a function of $\delta_1/t_1$, the ratio of skin

depth $\delta_1$ in the upper layer to upper-layer thickness $t_1$, where the skin depth $\delta = \sqrt{2/\sigma\mu\omega}$. The conductivity contrast $\sigma_2/\sigma_1$ varies from 1/1,000 to 1,000. The panels show (a) the *inphase conductivity,* (b) the *phase conductivity,* (c) the *amplitude conductivity,* and (d) the *phase-amplitude conductivity* for a sensor with the following specifications: a coplanar coil-pair, a coil separation of 1.66 m and a sensor height of 1 m. In general, the apparent conductivity curves obtained from all of the four algorithms correctly indicate a two-layer case. When $\delta_1/t_1$ is small, the primary magnetic field is limited in the upper layer, so that the earth looks like a half-space with the upper-layer conductivity. The apparent conductivity is equal to the true conductivity of the upper layer. As $\delta_1/t_1$ increases, the primary field penetrates into the lower layer, and so the apparent conductivity approaches the value of the basement conductivity. The rate of approach to the basement conductivity is faster for the conductive basement than for the resistive basement. When $\delta_1/t_1$ is very large, the primary field deeply penetrates into the basement. The earth appears to be homogeneous with the conductivity of the basement, and values of apparent conductivity are equal to the true values of the basement conductivity, particularly when $\sigma_2/\sigma_1 > 1$.

There are some differences in the apparent conductivity curves obtained from the four methods. The *phase conductivity* of Fig. 4(b) has a greater variation and approaches the basement conductivity more rapidly at mid-values of $\delta_1/t_1$ than do the others, but it tends to underestimate $\sigma_2$, particularly at low conductivity contrasts. The amplitude-related conductivity curves [Figs. 4(c) and 4(d)] have the smallest range at mid-values of $\delta_1/t_1$ for the case of a conductive layer overlying resistive basement ($\sigma_2/\sigma_1 < 1$). However, the apparent conductivity continues to approach $\sigma_2$ for the larger conductivity contrasts, while the *inphase* and *phase conductivities* saturate at large $\delta_1/t_1$. The *phase-amplitude conductivity* of Fig. 4(d) behaves like the *amplitude conductivity* when $\sigma_2/\sigma_1 < 1$, and provides wide variation when $\sigma_2/\sigma_1 > 1$. Therefore, we would like to use the *phase-amplitude conductivity* because of good behavior and use of all available data.

We will now show how the apparent permeability behaves for magnetic two-layer cases with the magnetic permeability contrast $\mu_2/\mu_1$ from 1/100 to 100, but without conductivity contrast. Figure 5 shows the apparent permeability curves as a function of the ratio $\delta_1/t_1$. When $\delta_1/t_1$ is small (the upper layer is very thick compared to the skin depth in the upper layer), the lower layer makes no contribution to the EM response, so that the apparent permeability is equal to the true permeability of the upper layer. As $\delta_1/t_1$ increases (*i.e.,* the upper layer becomes thinner), the apparent permeability approaches the true values of the basement permeability. When $\delta_1/t_1$ is very large (*i.e.,* the thickness of the upper layer tends to zero), the apparent

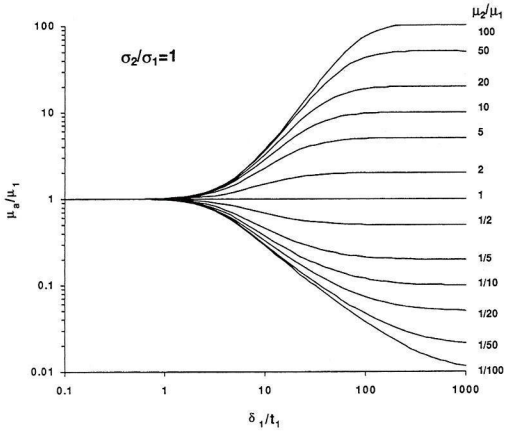


**Figure 5. The apparent permeability curves for a suite of two-layer models for the permeability ratios $\mu_2/\mu_1$ from 0.01 to 100.**

permeability is equal to the true value of the basement permeability.

The next example of synthetic data employs a suite of two-layer models with both permeability and conductivity contrast to show how the apparent permeability and apparent conductivity are affected. For simplicity, we deal only with the *phase-amplitude conductivity.* Let us consider four cases depending on the values of $\sigma_2/\sigma_1$ and $\mu_2/\mu_1$. One can imagine a coordinate system with an x-axis of $\sigma_2/\sigma_1$, y-axis of $\mu_2/\mu_1$, and its origin at (1, 1). In such a system, quadrants from the first to the fourth stand for the cases $\sigma_2/\sigma_1 > 1$ and $\mu_2/\mu_1 > 1$, $\sigma_2/\sigma_1 < 1$ and $\mu_2/\mu_1 > 1$, $\sigma_2/\sigma_1 < 1$ and $\mu_2/\mu_1 < 1$, and $\sigma_2/\sigma_1 > 1$ and $\mu_2/\mu_1 < 1$.

Figure 6 shows the apparent permeability curves for the four cases, the origin being assumed at the center of the four panels. The permeability contrast is fixed at 10, while the conductivity contrast varies. One can see that the apparent permeability is significantly affected by the conductivity contrast only in the first quadrant. When the conductivity contrast is small, the apparent permeability curves reach the value of basement permeability as $\delta_1/t_1$ increases. The values of apparent permeability underestimate the basement permeability, even for large $\delta_1/t_1$ as $\sigma_2/\sigma_1$ increases when $\mu_2/\mu_1 >> 1$. This phenomenon can be explained as follows: since both $\sigma_2$ and $\mu_2$ are high, as well as the effective value of $\sigma\mu f$, the ability to resolve the permeability is reduced, as shown in Fig. 3. In fact, the product $\sigma_2\mu_2 f$ is greater than 1 in these cases, therefore, the conductivity contrast will not significantly affect the apparent permeability if the effective value of $\sigma\mu f$ is low enough.

Figure 7 shows the apparent conductivity curves for the four cases. The conductivity contrast is fixed at 100,

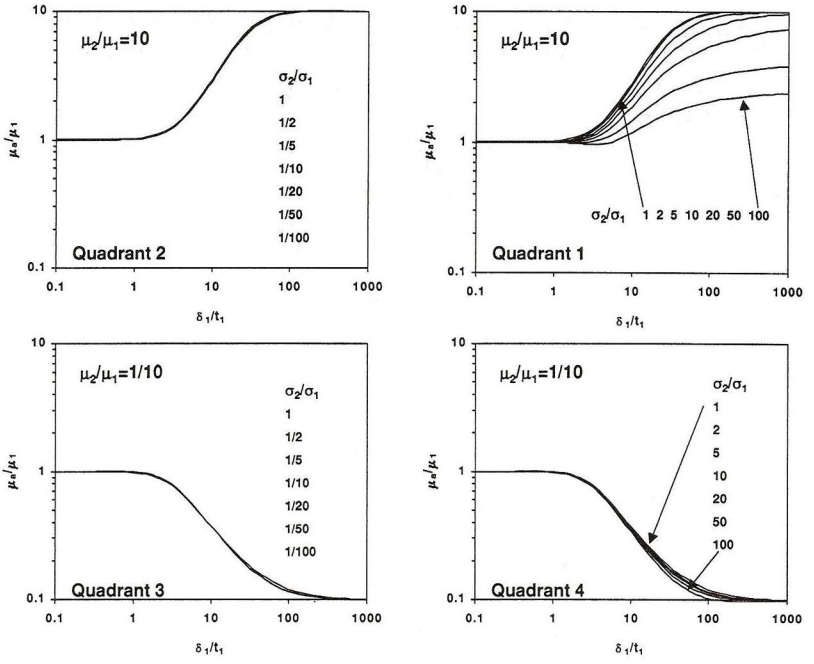


**Figure 6. The apparent permeability curves for a suite of two-layer models with a fixed permeability contrast $\mu_2/\mu_1$ of 10 and variable conductivity contrast.**

while the permeability contrast varies. The apparent permeability was computed first using Eq. 4; the apparent conductivity was then obtained from the EM data using the pre-computed apparent permeability. The apparent conductivity is significantly affected by the permeability contrast in the first and fourth quadrants. The curves in the first quadrant cannot approach the true value of basement conductivity for large values of $\delta_1/t_1$ because the apparent permeability cannot be well resolved. The conductivity curves in the fourth quadrant become dispersive in the transition zone, and the resolvability decreases with increasing permeability contrast, although all curves eventually reach the true basement conductivity. Also, the apparent conductivity is too low when difference between the two-layer permeability is large, as shown in the fourth quadrant. The apparent conductivity is only slightly affected in the second and third quadrants, where the lower layer is more resistive than the upper layer.

## Field Data Examples

Real data examples tend to encompass many permeability and conductivity variations in a single survey, particularly at urban, environmental sites. While apparent conductivity and apparent permeability may not always provide accurate estimates of the true material properties, they can at times provide a qualitative view of the variation of the electrical properties in the earth. To show the usefulness of this analytic method, we present three examples. These examples will use the GEM-2 sensor (Won *et al.,* 1996).

Our first example shows the results of the transformation from GEM-2 data obtained at a test site at Geophex in Raleigh, North Carolina. The survey area is 12 by 12 meters. In the center is a test well covered by a 30 cm diameter ferrous steel cap and, to the northwest, a 55-gallon steel drum with its top buried at 0.6m. GEM-2 data were acquired using a line spacing of 0.5 m. The apparent permeability is converted to susceptibility, using the equation $\kappa_a = \mu_{ra} - 1$, where $\kappa_a$ is apparent susceptibility and $\mu_{ra}$ is apparent relative permeability obtained from the EM data. Figure 8 presents maps of apparent susceptibility and apparent conductivity at 11,430 Hz. The anomalies of the two objects are clearly shown on both maps. The well cap causes a stronger susceptibility anomaly because it is on the surface. It is reasonable to ask whether such ferrous metals with a frequency as high as 11,430 Hz satisfies the condition $\sigma\mu f << 0.1$. Values of conductivity and permeability for ferrous metal objects are very high, but if their size is

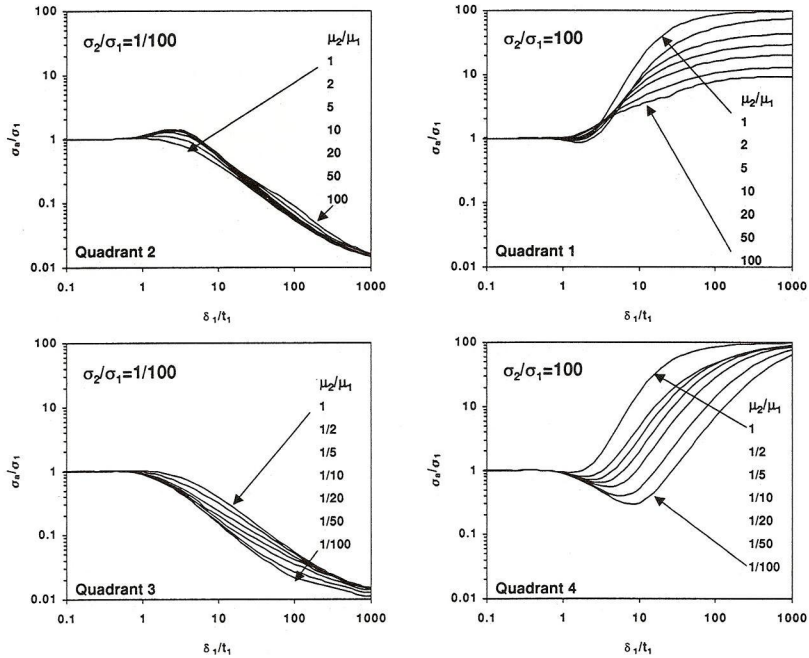


**Figure 7. The apparent conductivity curves for a suite of two-layer models with a fixed conductivity contrast $\sigma_2/\sigma_1$ of 100 and variable permeability contrast.**

small, their apparent permeability and conductivity computed from a half-space model will be much lower than their true values. Therefore, the half-space-equivalent $\sigma_a\mu_a f$ would be low enough to meet the condition. The values of apparent conductivity for the two objects are lower than the background conductivity because the EM response from an isolated object smaller and shallower than the GEM-2 coil separation is opposite in polarity from the background earth response. This can be seen from forward modeling based on a sphere model (Grant and West, 1965). A metal building nearby caused the conductivity high in the southwestern corner of the site.

Our second field example is from an old mirror manufacturing plant. Broken mirror pieces, also known as cullet, were stored above ground in a huge pile and, some years ago, were buried onsite. Subsequent site renovation that included paving completely concealed the burial site. The cullet contained lead-based paint, and leaching has eventually caused lead contamination in groundwater. The survey objective, therefore, was to locate the buried cullet and identify preferred drilling and chemical sampling locations.

A three-acre area was surveyed with a GEM-2, using a line spacing of 0.75 m. Data sampling along each line was approximately 0.3 m. The EM data were acquired using two frequencies simultaneously: 4,050 Hz and 12,270 Hz. Figure 9 presents maps of the apparent susceptibility and apparent conductivity. The apparent permeability is calculated from both the measured inphase and quadrature data; the computed permeability is then used to obtain apparent conductivity. The buried cullet is identifiable at both frequencies. The area of conductivity high for 4,050 Hz is larger than that for 12,270 Hz, indicating the contaminant plume is larger at depth than near the surface. The linear features delineate the known water, sewer, and underground power lines. Isolated features are associated with metallic objects, industrial debris, manholes, hydrant and storm water grates, and barrels.

The last field example is from a defunct Manufactured Gas Plant (MGP) in New England. The objectives of the survey included identifying and locating any remaining building foundations, abandoned pipelines, isolated objects, and potential contaminant sources and impacted areas. We acquired GEM-2 and magnetic data over the three-acre site along transects spaced 0.75 m apart. GEM-2 operated at three simultaneous frequencies: 1,050 Hz, 7,290 Hz, and 18,270 Hz.

Figure 10 shows the total magnetic field and the ap-

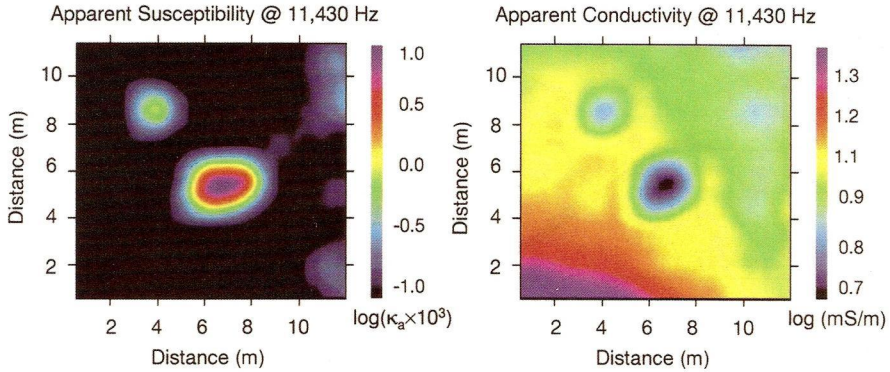


**Figure 8. Maps of (a) the apparent susceptibility and (b) apparent conductivity computed from the GEM-2 data (11,430 Hz) observed at Geophex testing site.**

parent susceptibility map obtained from the 1,050 Hz EM data. The apparent susceptibility map of Fig. 10(b) looks somewhat different from the corresponding total field magnetic map of Fig. 10(a). The differences can be attributed to several factors. First, the EM and magnetometer sensors sample quite different geology due to their different depths of exploration. Thus, the EM data reflect only the near-surface magnetic properties while the magnetometer sees deeper. Second, the EM data produce inherently higher spatial resolution than the magnetic data. Third, the EM sensor responds only to induced magnetization while a magnetometer responds to both induced and remnant magnetization. Fourth, the EM method may miss the magnetic property of a magnetic object if it is highly conductive at the transmit-

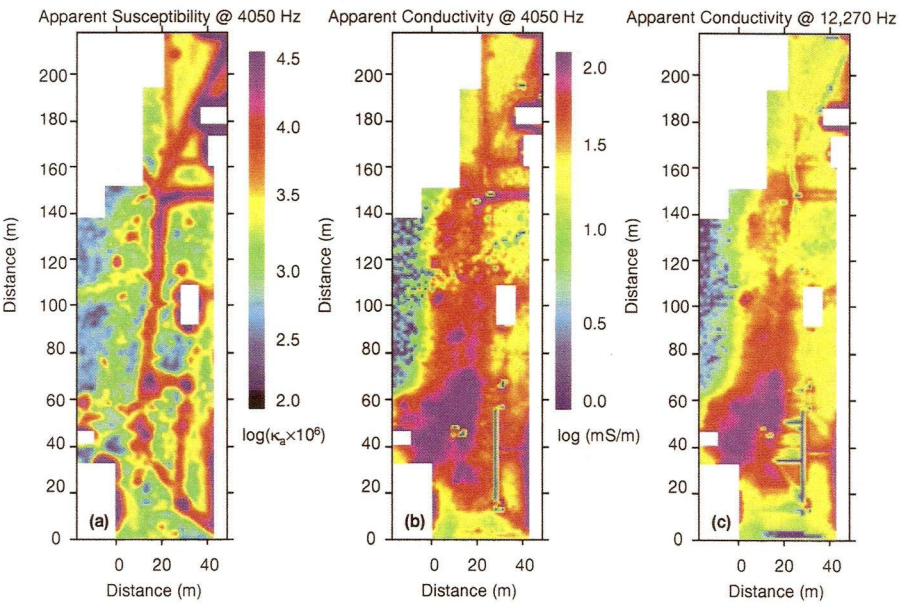


**Figure 9. The results from a GEM-2 survey at Mirrors-R-Us site showing: (a) the magnetic susceptibility calculated from the 4,050 Hz GEM-2 EM data, and the apparent conductivity maps obtained from (b) the 4,050 Hz data and (c) the 12,270 Hz data.**

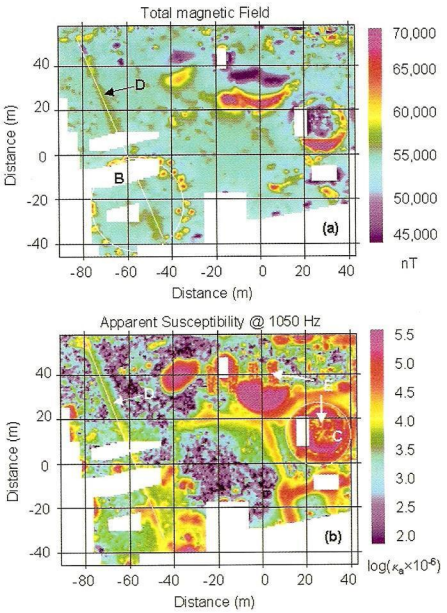


←

**Figure 10. The results from a GEM-2 survey at MGP site showing: (a) the static total magnetic field as measured by a magnetometer, and (b) the magnetic susceptibility calculated from the 1,050 Hz GEM-2 electromagnetic data.**

ting frequency, whereas the magnetometer responds only to the static magnetization. The features shown on the magnetic and conductivity maps are discussed below.

Figure 11 presents the apparent conductivity maps at the three frequencies. Prominent anomalies include several large circular features that correspond to the known building foundations. Two of the circles (A and B) possess high conductivity and susceptibility in the center. These central conductivity and susceptibility highs probably represent metal-reinforcement located beneath the structure. The total magnetic field map of Fig. 10(a) indicates clearly two (B and C) of the circular features, one of which is observed on the apparent susceptibility map (C).

A distinct change in the apparent conductivity coinciding with the storm sewer (D) in the western portion of the site can also be seen. The storm sewer is seen as a linear feature in the magnetic data and apparent susceptibility data

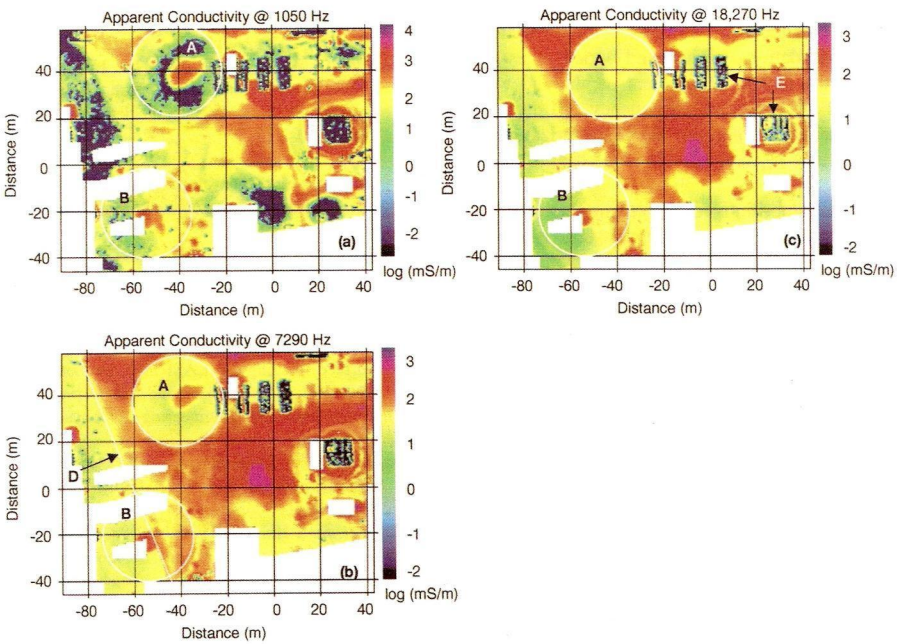


**Figure 11. Apparent conductivity maps for (a) 1,050 Hz, (b) 7,290 Hz, and (c) 18,270 Hz. The map area is the same area as for Fig. 10.**

of Fig. 10. It is also seen on the conductivity maps as a boundary between two different zones (Fig. 11). Based on the conductivity, it appears that the near-surface materials east of the storm sewer are distinctly different from those to the west of the sewer. The storm sewer location represents a former geographic boundary; the western side is a fill area. Thus, the contact zone causes a large anomaly masking the linear conductivity anomaly from the storm sewer itself.

Several linear features and numerous isolated anomalies are observed throughout the site. Gas lines connected to the MGP buildings are most likely the cause of several linear conductivity and susceptibility highs in the southeastern part of the site, as shown in Figs. 10 and 11. The isolated anomalies probably result from buried industrial waste associated with demolition of the facility.

Five rectangular conductivity lows and susceptibility highs (E) are present in the northeastern portion of the site. These features are not present in the total magnetic field map. Although two of these anomalies coincide with visible concrete sections on the surface, there is no surface indication of the other three. These susceptibility highs probably represent reinforced wires in the concrete.

## Conclusions

Apparent conductivity and susceptibility mapping is a non-intrusive, rapid, and cost effective technique for identifying building foundations, piping, and buried industrial waste. To detect the objects at different depths and with different electrical properties, multifrequency EM data are required to adequately complete the site characterization. It is therefore important to measure a bandwidth as wide as possible.

We developed algorithms for converting the multifrequency EM data to the apparent conductivity and apparent permeability based on the magnetic and conductive halfspace model. The apparent permeability is first estimated from the amplitude and phase data at a low frequency. Using the apparent permeability thus obtained, we proceed to compute apparent conductivity from the EM data at all survey frequencies. The apparent conductivity may be computed from five algorithms based on the input data. In general, three of the five algorithms yield unique solutions; they are *inphase conductivity, phase conductivity,* and *phase-amplitude conductivity.* Among the three algorithms, we prefer to use *phase-amplitude conductivity* in practice, since it is stable and uses all available data. The algorithm for *amplitude conductivity* yields a unique solution when the relative permeability is less than two. The *quadrature* algorithm gives a unique solution at the low or high values of $\sigma\mu f$, but gives a double-value at the middle range. Determination of apparent permeability is virtually independent of the conductivity contrast if the condition $\sigma\mu f << 0.1$ is satisfied; however, the permeability contrast would affect the behavior of the apparent conductivity, especially in the case of a resistive layer overlying conductive basement.

The field examples show that the GEM-2 EM mapping successfully identified the buried cullet, abandoned building foundations, piping, and buried materials.

## Acknowledgment

This study has been partly funded by the Department of Defense Environmental Security Technology Certification Program (ESTCP) in Arlington, Virginia, and Naval Research Laboratory in Washington, D.C.

## References

Fraser, D.C., 1978, Resistivity mapping with an airborne multicoil electromagnetic system: Geophysics, **43**, 144–172.

Frischknecht, F.C., 1967, Fields about an oscillating magnetic dipole over a two-layer earth and application to ground and airborne electromagnetic surveys: Quarterly of the Colorado School of Mines, **62**, No.1, 326.

Grant, F.S., and West, G.F., 1965, Interpretation theory in applied geophysics, McGraw-Hill Book Co., New York.

Huang, H., and Fraser, D.C., 1998, Magnetic permeability and electrical conductivity mapping with a multifrequency airborne EM system: Exploration Geophysics, **29**, 249–253.

Huang, H., and Fraser, D.C., 2000, Airborne resistivity and susceptibility mapping in magnetically polarizable areas: Geophysics, **65**, 502–511.

Keiswetter, D., Novikova, E., Won, I.J., Hall, T., and Hanson, D., 1997, Development of a monostatic, multifrequency electromagnetic mine detector: Society of Optical Engineering, **3079**, 831–839.

Keiswetter, D.A., and Won, I.J., 1997, Multifrequency electromagnetic signature of the Cloud Chamber, Nevada Test Site, Journal of Environmental and Engineering Geophysics, **2**, No.2, 99–104.

Murray, C., and Keiswetter, D., 1998, Application of magnetic and multi-frequency EM techniques for landfill investigations: Case histories: SAGEEP Conference Proceedings, 445–452.

Sternberg, B.K., and Birken, R.A., 1999, A new method of subsurface imaging-the LASI high frequency Ellipticity system: part 3. system tests and field surveys: Journal of Environmental and Engineering Geophysics, **4**, No.4, 227–240.

Ward, S.H., 1967, Electromagnetic theory for geophysical applications: *in* Ward, S.H., Ed., Mining Geophysics, Society of Exploration Geophysicists, Theory, 13–196.

Ward, S.H., and Hohmann, G.W., 1988, Electromagnetic theory for geophysical applications: *in* Nabighian, M.N., Ed., Electromagnetic Methods in Applied Geophysics, Society of Exploration Geophysicists, Theory, 130–311.

Witten, A.J., and Calvert, G., 1999, Characterizing the distribution of near-surface solution channels using electromagnetic induction and ground penetrating radar: Journal of Environmental and Engineering Geophysics, **4**, No. 1, 35–43.

Won, I.J., Keiswetter, D., Fields, G., and Sutton, L., 1996, GEM-2: A new multifrequency electromagnetic sensor: Journal of Environmental and Engineering Geophysics, **1**, No. 2, 129–137.

Won. I.J., Keiswetter, D., Hanson, D., Novikova, E., and Hall, T., 1997, GEM-3: A monostatic broadband electromagnetic induction sensor: Journal of Environmental and Engineering Geophysics, **2**, No. 1, 53–64.

Won, I.J., Keiswetter, D., and Novikova, E., 1998, Electromagnetic induction spectroscopy: Journal of Environmental and Engineering Geophysics, **3**, No. 1, 27–40.